Stability and mixing of shear layers forced by standing internal waves

Alexis Kaminski and John Taylor

Department of Applied Mathematics & Theoretical Physics,
University of Cambridge
A.K.Kaminski@damtp.cam.ac.uk

Abstract

Turbulence generated by breaking internal waves is an important source of mixing in the ocean interior, and is often interpreted in terms of the stability of the vertical shear. However, observations and numerical studies suggest that vertical internal wave strain may also play a key role in stratified flow stability. Here we model the effects of wave strain by imposing a spatially- and temporally-periodic standing wave onto a stably-stratified shear flow. To examine the linear stability of this flow, we compute optimal perturbations for a range of target times, wave amplitudes, and stratifications. The standing wave catalyzes perturbation growth in the shear layer, leading to enhanced energy gains. We then perform direct numerical simulations to examine the nonlinear perturbation evolution. We find that in some cases the linear growth is sufficient to trigger nonlinear effects and transition to turbulence. The mixing efficiency varies in time with the background wave, suggesting that the phase of the flow may be an important parameter in describing the mixing.

1 Introduction

Vertical mixing in the stably-stratified ocean interior is thought to be a key player in setting the vertical density structure and distributions of tracers which are important for climate and biogeochemical cycles. However, the turbulent eddies responsible for mixing are typically on the order of several meters in size, and are unresolved in ocean circulation models. Parameterizations of the physics leading to mixing are therefore required.

Mixing is often assumed to arise in the ocean interior as the result of shear instabilities. The Miles-Howard theorem states that, for parallel, steady, inviscid stratified shear flows, a necessary condition for instability is that the gradient Richardson number be less than 1/4 somewhere in the domain. This concept has been used as the basis of several mixing parameterizations (e.g. Mellor and Yamada, 1982; Price et al., 1986). Theoretical and numerical work has suggested other linear mechanisms by which perturbations may grow and lead to mixing in linearly stable flows (Farrell and Ioannou, 1993; Kaminski et al., 2014). Additionally, and perhaps more relevant to the question of ocean mixing, is the fact that geophysical flows are rarely parallel and steady – assumptions which are key in the Miles-Howard theorem.

Oceanic observations of overturns and dissipation suggest that shear and gradient Richardson number alone may not be the entire story in determining regions of enhanced mixing. Increasingly, there is evidence that vertical strain, γ (the normalized distance between adjacent isopycnals), and the vertical strain rate, $1/\gamma\,\partial\gamma/\partial t \approx \partial w/\partial z$, may also play an important role in mixing events (Alford and Pinkel, 2000; Aucan et al., 2006; Levine and Boyd, 2006). In addition to oceanic observations, there is numerical evidence for mixing induced by vertical strain in stratified flows. For example, in their numerical simulations of stratified turbulence forced by large-scale standing internal waves, Carnevale et al. (2001) observe the development of small-scale vertical "spouts" in regions of strong

straining motion. The growth and subsequent collapse of these spouts lead to local zones of mixed fluid.

This past work points to internal wave strain being important for the dynamics of stably-stratified shear flows and motivates the current research. As in Carnevale et al. (2001), we consider the stability of a stratified flow forced by a standing internal wave, but here we include a parallel hyperbolic-tangent shear flow. To examine the stability of this flow we consider both the linear stability by identifying the structures which grow the most over finite time horizons, and the resulting nonlinear behaviour and mixing by performing full direct numerical simulations of the computed perturbations. We focus primarily on the behaviour of the shear layer, rather than the large-scale standing wave as seen in Carnevale et al. (2001). By considering this idealized but still spatially- and temporally-varying flow, we hope to identify the most relevant physical processes, which may then be useful in developing future parameterizations of ocean mixing.

2 Problem setup and implementation

We begin with a hyperbolic-tangent shear profile and uniform background stratification, given in dimensional form by $U^*(z^*) = U_0^* \left[\tanh\left(z^*/h^* - L_z^*/2h^*\right)\right]$ and $B^*(z^*) = N_0^{*2} z^*$. We nondimensionalize lengths by h^*, times by h^*/U_0^*, velocities by U_0^*, and buoyancy by $N_0^{*2}h^*$. The nondimensional shear profile is then $U_s(z) = \tanh\left(z - L_z/2\right)$. We also define the Reynolds, Prandtl, and bulk Richardson numbers for this flow as $Re = U_0^* h^*/\nu^*$, $Pr = \nu^*/\kappa^*$, and $Ri_b = N_0^{*2} h^{*2}/U_0^{*2}$, respectively, where ν^* and κ^* are the viscosity and diffusivity of the fluid.

We model the effect of internal wave strain by defining an inviscid, non-diffusive standing internal wave acting in the yz-plane using second-order expressions based on those given by Thorpe (1968),

$$\begin{aligned} U(y,z,t) =& U_s - AU_s' \sin k_{zw} z \cos\omega t \cos k_{yw} y + \frac{A^2 k_{zw}}{8} U_s' \sin 2k_{zw} z (1 + \cos 2\omega t) \\ &+ \frac{A^2}{8} U_s'' \sin^2 k_{zw} z (1 + \cos 2\omega t - (1 - \cos 2\omega t)\cos 2k_{yw} y)\,, \end{aligned} \tag{1}$$

$$V(y,z,t) = \frac{A\omega k_{zw}}{k_{yw}} \sin(\omega t + \phi) \sin k_{yw} y \cos k_{z,w}\,, \tag{2}$$

$$W(y,z,t) = -A\omega \sin(\omega t + \phi) \cos k_{yw} y \sin k_{zw} z\,, \tag{3}$$

$$B(y,z,t) = z - A \sin k_{zw} z \cos\omega t \cos k_{yw} y + \frac{A^2 k_{zw}}{8} \sin 2k_{zw} z (1 + \cos 2\omega t)\,. \tag{4}$$

where A is a wave amplitude (normalized by h^*) and $k_{yw} = 2\pi/L_y$ and $k_{zw} = 2\pi/L_z$ are the horizontal and vertical wavenumbers of the wave, respectively. Primes denote $\mathrm{d}/\mathrm{d}z$. The natural internal wave frequency ω, given k_{yw} and k_{zw}, is defined by $\omega/\sqrt{Ri_b} = k_{yw}/\sqrt{k_{yw}^2 + k_{zw}^2}$. The expressions given above for the standing wave are expected to be valid in the limit where $Ak_{zw} \ll 1$ (Thorpe, 1968).

The combination of the standing wave and the shear flow leads to a base flow that varies in both space and time in all three components of velocity $\mathbf{U}(y,z,t)$ and buoyancy $B(y,z,t)$, as illustrated schematically in figure 1(a). The standing wave alternately compresses and expands both the isopycnals and background shear in the yz-plane, leading to lower values of the local gradient Richardson number in the compressed regions (and increased values in the expanded regions). This occurs despite the locally-stronger stratification as a result of the corresponding strengthening of the local shear.

Figure 1(b) shows the minimum gradient Richardson number of the background flow as a function of A and Ri_b. It is clear that stronger background standing waves lead to a lower $Ri_{g,min}$ for the flow, and in some cases may decrease $Ri_{g,min}$ below the critical value of 1/4 predicted by the Miles-Howard theorem (Miles, 1961; Howard, 1961). (Note, however, that the base flow considered here is neither parallel nor steady, thus calling into question the applicability of the Miles-Howard result).

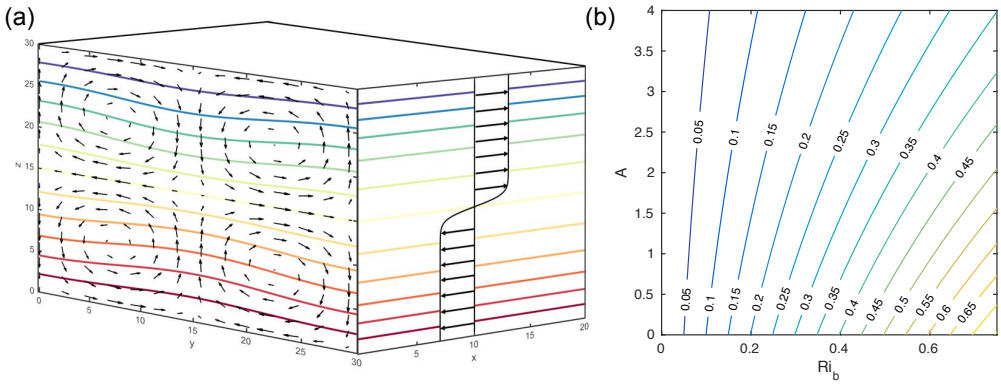

Figure 1: (a) Schematic of background flow. Arrows denote velocities and contours denote buoyancy. (b) Minimum gradient Richardson numbers attained by the background flow defined by (1)-(4) as a function of the wave amplitude A and bulk Richardson number Ri_b.

3 Linear results

To examine the stability of the base flow given by equations (1)-(4), we seek the linear optimal perturbations, i.e. the initial conditions $\mathbf{u}_0$ and b_0 which maximize the linear perturbation energy gain for a given target time T. The gain is defined by

$$G(T) = \frac{\frac{1}{2}(\langle \mathbf{u}(T), \mathbf{u}(T)\rangle + Ri_b\langle b(T), b(T)\rangle)}{\frac{1}{2}(\langle \mathbf{u}_0, \mathbf{u}_0\rangle + Ri_b\langle b_0, b_0\rangle)}, \tag{5}$$

where $\mathbf{u}$ is the perturbation velocity, b is the perturbation buoyancy, and the angle brackets define the inner product $\langle \mathbf{f}, \mathbf{g}\rangle = 1/V \int_V \mathbf{f}\cdot\mathbf{g}\,\mathrm{d}V$. We apply the direct-adjoint looping approach in order to solve for the optimal perturbations (described in Kaminski et al. (2014) and Kaminski (2016)), which allows for consideration of complicated base flows and does not rely on any assumption of slow variation of properties in time or space.

We calculate linear optimal perturbations for three bulk Richardson numbers (Ri_b = 0.30, 0.40, and 0.50) and five wave amplitudes (A = 0.50, 1.50, 2.50, and 3.50, as well as the case with no wave, A = 0.00). For these choices of A and Ri_b, $Ri_{g,min}$ is less than 1/4 for $A > 1.50$ when $Ri_b = 0.30$ and for $A > 2.50$ when $Ri_b = 0.40$ as shown by figure 1(b). Four target times are considered, corresponding to half, one, one and a half, and two periods of the background standing wave (i.e. $T = \pi/\omega$, $2\pi/\omega$, $3\pi/\omega$, and $4\pi/\omega$ for each value of Ri_b). The initial background flow corresponds to the time of maximum isopycnal deflection. The domain size is $(L_x, L_y, L_z) = (20.0, 30.0, 30.0)$, and the standing wave has $k_{yw} = k_{zw} = 2\pi/30.0$ (i.e. an aspect ratio of one). For simplicity, we keep the Reynolds and Prandtl numbers fixed at $Re = 1000$ and $Pr = 1$, respectively.

The vertical velocities of the optimal perturbations corresponding to $Ri_b = 0.40$ and $A = 1.50$ are shown in figure 2 for $T = \pi/\omega$ and $T = 2\pi/\omega$. Also shown for comparison

is the optimal perturbation for the same target times with $A = 0.00$. The primary effect of the standing wave on the structure of the optimal perturbation is to localize it in the y-direction in regions of high vertical strain rate, as shown by figures 2(b) and (d). In particular, the perturbations localize such that they benefit from the effects of vertical compressive strain during their evolution, as discussed below. Within the localized region, the structure of the optimal perturbations in the xz-plane is similar to that of the perturbations for the shear layer alone, namely a series of rolls tilted against the background shear flow as required for energy growth via the Orr mechanism (Orr, 1907).

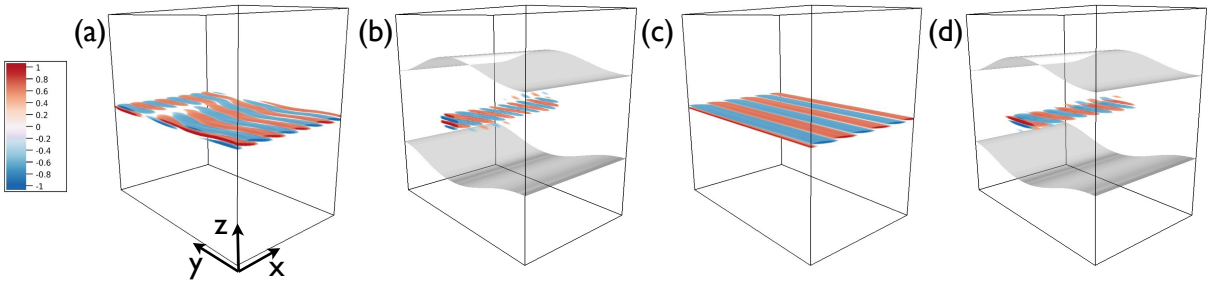

Figure 2: Structure of computed linear optimal perturbations for short target times. The colours denote the perturbation vertical velocities, and the isosurfaces show the background buoyancy field. (a) $A = 0.00$ and $T = \pi/\omega$. (b) $A = 1.50$ and $T = \pi/\omega$. (c) $A = 0.00$ and $T = 2\pi/\omega$. (d) $A = 1.50$ and $T = 2\pi/\omega$. $Ri_b = 0.40$ for all cases shown here.

Figure 3 shows the computed optimal mean growth rate $\sigma_m(T) = \ln G(T)/2T$. The perturbation energy growth may be substantially increased in the presence of standing waves compared to the unstrained case ($A = 0.00$). At longer times, the mean growth rates plateau as the normal-mode instability associated with the standing wave dominates (Bouruet-Aubertot et al., 1995), but much higher mean growth rates $\sigma_m(T)$ are found at shorter times. This is in agreement with the observation in Kaminski et al. (2014) where perturbations to base flows that allowed for Kelvin-Helmholtz instability still attained higher growth rates than the predicted normal-mode growth rates at shorter T. It is worth noting that the $\mathcal{O}(0.1)$ growth rates are of the same order as the background forcing frequency (where $\omega \sim 0.4 - 0.5$), indicating that the perturbations evolve on a similar timescale to the variation of the background flow. Thus, the frozen-in-time approach commonly used in linear stability analysis would not have been justified here.

By examining the details of the perturbation energy budget (not presented here), it can be shown that the enhanced linear perturbation energy gain arises due to an enhancement of the existing shear-based transient growth mechanism for unstrained flows (Kaminski et al., 2014). That is, the vertical internal wave strain acts to catalyze perturbation growth via shear.

4 Nonlinear results

Given the significant linear perturbation energy gain, it is natural to ask whether the optimal perturbations computed in the previous section would be susceptible to nonlinear effects. To examine this question, we carry out direct numerical simulations by solving the full Boussinesq Navier-Stokes and buoyancy conservation equations governing the evolution of perturbations $\mathbf{u}$ and b for a prescribed background flow $\mathbf{U}$ and B.

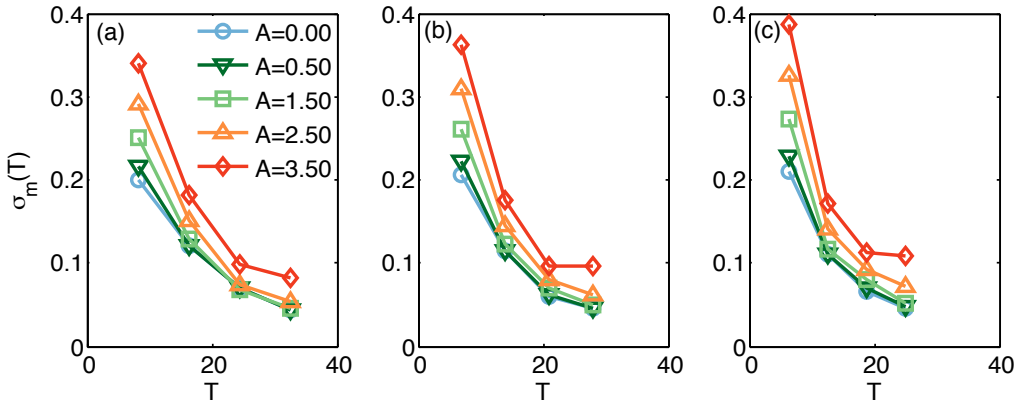

Figure 3: Mean perturbation growth rate, $\sigma_m(T)$, as a function of target time T and standing wave amplitude A. (a) $Ri_b = 0.30$. (b) $Ri_b = 0.40$. (c) $Ri_b = 0.50$.

The governing equations are solved in the framework of DIABLO (Taylor, 2008). The horizontal directions are periodic in space and treated pseudospectrally, while the vertical direction employs a second-order finite-difference discretization. The vertical grid is clustered around the centre of the shear layer. At the top and bottom of the domain, a sponge layer is used to mimic open boundaries.

The linear optimal perturbations corresponding to a target times of half and one forcing period are used as initial conditions for the simulations. The initial perturbation amplitude set to $E_0 = 5 \times 10^{-6}$ for all simulations, and random noise with an amplitude of 1/10 of E_0 is superposed onto the initial perturbation. We consider cases with $A = 1.50$ and $Ri_b = 0.30$, 0.40, and 0.50 and an additional case with $A = 2.50$ and $Ri_b = 0.40$. The details of the simulations are summarized in table 1.

Table 1: Details of direct numerical simulations run with and without an added background standing wave.

A	Ri_b	T	(N_x, N, N_z)
0.00	0.30	π/ω, $2\pi/\omega$	(256,256,201), (256,256,201)
0.00	0.40	π/ω, $2\pi/\omega$	(256,256,201), (192,192,201)
0.00	0.50	π/ω, $2\pi/\omega$	(192,192,201), (192,192,201)
1.50	0.30	π/ω, $2\pi/\omega$	(384,384,301), (384,384,301)
1.50	0.40	π/ω, $2\pi/\omega$	(384,384,301), (384,384,301)
1.50	0.50	π/ω, $2\pi/\omega$	(256,256,201), (256,256,201)
2.50	0.40	$2\pi/\omega$	(384,384,301)

In some cases the optimal perturbations lead to strong nonlinearity and the development of secondary instabilities. For example, figure 4 shows an isosurface of constant buoyancy passing through the centre of the shear layer for $Ri_b = 0.30$, $A = 1.50$, and a perturbation computed for a target time $T = \pi/\omega$. The perturbation is first tilted upward by the background shear and forms an array of billows in the direction of the background shear. Eventually, a spanwise secondary instability develops on the billows and the billow begins to break down to smaller scales. This leads to the development of a turbulent region which is confined in the y-direction, and which eventually decays at longer times.

The total nonlinear perturbation energy evolution with respect to time, $E(t) = \langle \mathbf{u}, \mathbf{u} \rangle + Ri_b \langle b, b \rangle$, is shown by the dashed lines in figure 5(c) for $A = 0.00$, $A = 1.50$, and $A = 2.50$,

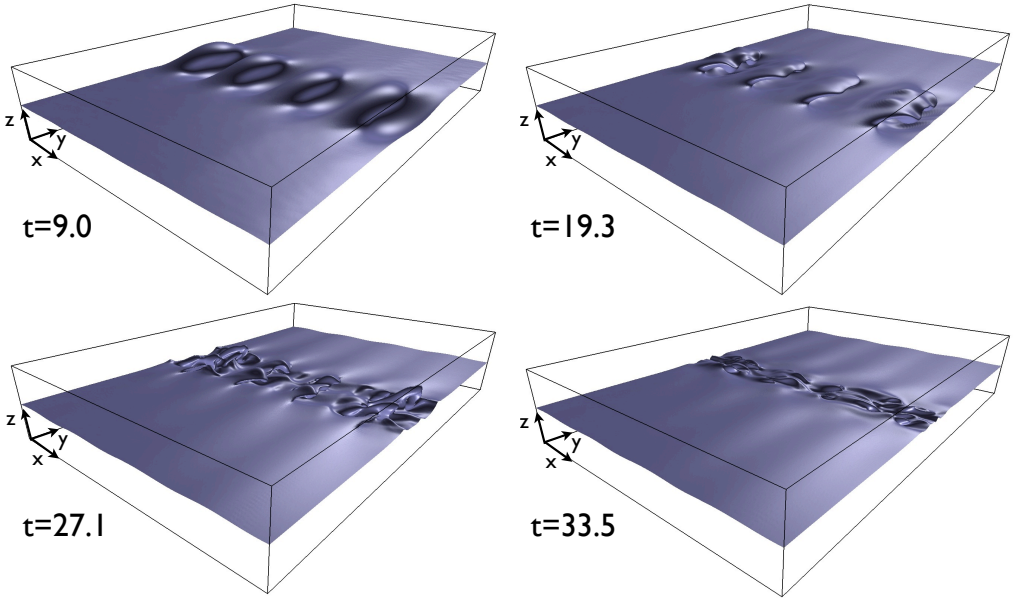

Figure 4: Isosurface of total buoyancy, $B+b$, passing through the centre of the shear layer. The simulation shown has $Ri_b = 0.30$, $A = 1.50$, with an initial perturbation corresponding to a target time of π/ω. The aspect ratio has been stretched by a factor of two in the vertical to better show the details of the perturbation evolution.

a target time of one forcing period, and $Ri_b = 0.40$. Figure 5(c) also shows the corresponding energy evolution in the case where the perturbation is unaffected by nonlinearity (solid lines). The initial perturbation energy evolution follows closely the linear evolution, indicating that the energy growth at early times corresponds to the linear non-normal growth described in the previous section. Later, the nonlinear energy evolution deviates from the linear prediction. Eventually, the growth saturates at a peak value less than the theoretical linear energy maximum. This saturation is more apparent in the flows where the perturbation experiences higher energy gain ($A = 1.50$ and especially $A = 2.50$). This may be a function of the larger gains experienced by the perturbations in the presence of the background standing wave, but may also be an effect of the localization of the perturbation: for a given initial energy amplitude, the associated perturbation velocities $\mathbf{u}$ and buoyancy b are expected to be larger than in the case where the perturbation fills the entirety of the shear layer (see figure 2).

As mentioned in the introduction, a key quantity of interest in stratified shear flows is the mixing. Here, we quantify the efficiency of mixing by comparing the amount of energy used in dissipating potential energy to the total amount of dissipation in the flow, $\eta = \varepsilon_p/(\varepsilon_k + \varepsilon_p)$, where ε_k and ε_p are the dissipation of kinetic and potential energy respectively, defined as

$$\varepsilon_k = \frac{1}{V}\int_V \frac{1}{Re}\frac{\partial u_i}{\partial x_j}\frac{\partial u_i}{\partial x_j}\,\mathrm{d}V \qquad \text{and} \qquad \varepsilon_p = \frac{1}{V}\int_V \frac{Ri_b}{RePr}\frac{\partial b}{\partial x_j}\frac{\partial b}{\partial x_j}\,\mathrm{d}V\,. \tag{6}$$

Figure 5(d) shows the time evolution of the mixing efficiency, $\eta(t)$, for a background flow with no standing wave ($A = 0.00$) and one with a standing wave with $A = 2.50$. For both cases, there is an initial decrease due to the decay of the additive noise. This is followed by a period of strong increase in mixing efficiency up to values as high as approximately 0.65 as the perturbation grows, similar to the observed evolution of mixing

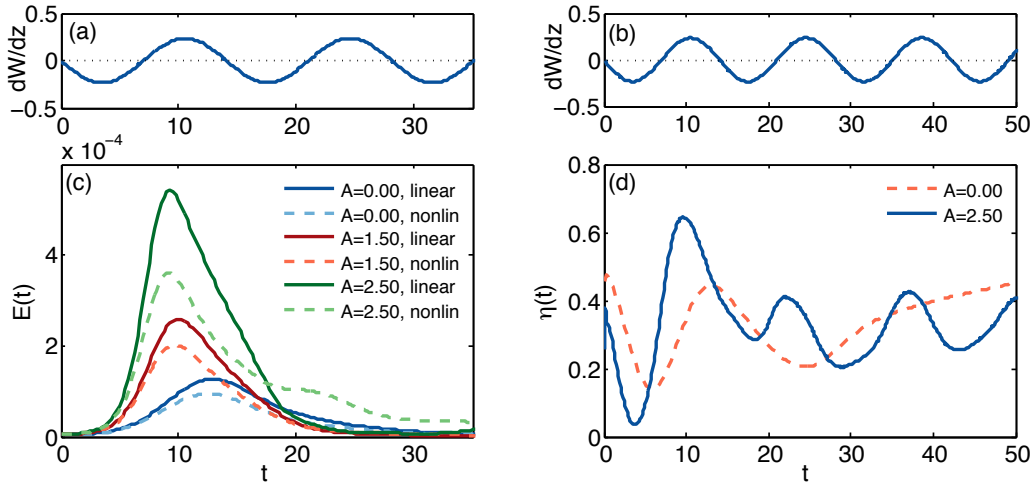

Figure 5: (a),(c) Background vertical strain rate, $\partial W/\partial z$, through the centre of the perturbation ($y = L_y/2$, $z = L_z/2$). (b) Time evolution of total perturbation energy $E(t)$ for linear (solid) and nonlinear (dashed) simulations. The blue lines correspond to $A = 0.00$, the red lines to $A = 1.50$, and the green lines to $A = 2.50$. (d) Time evolution of mixing efficiency, $\eta(t)$, for $A = 0.00$ and $A = 2.50$. The cases shown have $Ri_b = 0.40$ and $T = 2\pi/\omega$.

efficiency for Kelvin-Helmholtz instability (Peltier and Caulfield, 2003). As the perturbations continue to evolve, the mixing efficiency decreases to a value of approximately 0.3. However, the influence of the background flow is apparent, with increasing mixing efficiency during times of compressive vertical strain rate ($\partial W/\partial z < 0$). This is in contrast to the unstrained flow for which the mixing efficiency is tending towards a constant value after the initial transient evolution.

5 Conclusions

Here we have computed the linear optimal perturbations corresponding to a base flow consisting of a parallel, steady stratified shear flow interacting with a large-scale standing internal wave, based on the expressions given by Thorpe (1968). The straining flow associated with the internal wave acts to alternately compress and expand the shear layer, modifying the shear and stratification in space and in time.

Over time horizons of the order of one wave period, the added standing wave increases the maximum perturbation energy gain by up to an order of magnitude, with higher increases observed for larger-amplitude waves. In contrast to the optimal perturbations computed for the stratified shear layer alone, the perturbations to the strained flow localize in regions of high-amplitude vertical strain rate, $\partial W/\partial z$. In the presence of compressive strain ($\partial W/\partial z < 0$), the growth of perturbation energy via vertical shear production is enhanced, leading to higher perturbation energy growth via the shear-based Orr mechanism. At longer target times, there is a shift in the growth mechanism favoured by the optimal perturbations to the normal-mode instability of the standing wave.

We have also performed complementary direct numerical simulations, initialized by giving the computed optimal perturbations a small but finite initial amplitude. The perturbations grow linearly before saturating at larger amplitudes. The energy growth is sufficient to cause strongly nonlinear effects such as the development of billows, and for certain parameters the flow transitions to turbulence. Mixing efficiencies vary in time

with the background straining flow, suggesting that the phase of the turbulent event is an additional factor in determining the associated mixing efficiency.

References

Alford, M. H. and Pinkel, R. (2000). Observations of overturning in the thermocline: the context of ocean mixing. *J. Phys. Oceanogr.*, 30:805–832.

Aucan, J., Merrifield, M. A., Luther, D. S., and Flament, P. (2006). Tidal mixing events on the deep flanks of Kaena Ridge, Hawaii. *J. Phys. Oceanogr.*, 36:1202–1219.

Bouruet-Aubertot, P., Sommeria, J., and Staquet, C. (1995). Breaking of standing internal gravity waves through two-dimensional instabilities. *J. Fluid Mech.*, 285:265–301.

Carnevale, G. F., Briscolini, M., and Orlandi, P. (2001). Buoyancy- to inertial-range transition in forced stratified turbulence. *J. Fluid Mech.*, 427:205–239.

Farrell, B. F. and Ioannou, P. J. (1993). Transient development of perturbations in stratified shear flow. *J. Atmos. Sci.*, 50(14):2201–2214.

Howard, L. N. (1961). Note on a paper of John W. Miles. *J. Fluid Mech.*, 10:509–512.

Kaminski, A. K. (2016). *Linear optimal perturbations and transition to turbulence in strongly stratified shear flows*. PhD thesis, University of Cambridge.

Kaminski, A. K., Caulfield, C. P., and Taylor, J. R. (2014). Transient growth in strongly stratified shear layers. *J. Fluid Mech.*, 758:R4.

Levine, M. D. and Boyd, T. J. (2006). Tidally forced internal waves and overturns observed on a slope: results from HOME. *J. Phys. Oceanogr.*, 36:1184–1201.

Mellor, G. L. and Yamada, T. (1982). Development of a turbulence closure model for geophysical fluid problems. *Rev. Geophys. Space Phys.*, 20(4):851–875.

Miles, J. W. (1961). On the stability of heterogeneous shear flows. *J. Fluid Mech.*, 496:496–508.

Orr, W. M. (1907). The stability or instability of the steady motions of a perfect liquid and of a viscous liquid. Part I: A perfect liquid. *Proc. R. Irish Acad. A*, 27:9–68.

Peltier, W. R. and Caulfield, C. P. (2003). Mixing efficiency in stratified shear flows. *Annu. Rev. Fluid Mech.*, 35:135–167.

Price, J. F., Weller, R. A., and Pinkel, R. (1986). Diurnal cycling: Observations and models of the upper ocean response to diurnal heating, cooling, and wind mixing. *J. Geophys. Res.*, 91(C7):8411–8427.

Taylor, J. R. (2008). *Numerical simulations of the stratified oceanic bottom boundary layer*. PhD thesis, University of California, San Diego.

Thorpe, S. A. (1968). On standing internal gravity waves of finite amplitude. *J. Fluid Mech.*, 32(3):489–528.